Journal of Alloys and Compounds 509 (2011) 3065–3069

Contents lists available at ScienceDirect

Journal of Alloys and Compounds

journal homepage: www.elsevier.com/locate/jallcom

Epitaxial $0.65PbMg_{1/3}Nb_{2/3}O_3$–$0.35PbTiO_3$ (PMN–PT) thin films grown on $LaNiO_3/CeO_2$/YSZ buffered Si substrates

Juan Jiang [a], Soon-Gil Yoon [a,b,*]

[a] School of Nano Science and Technology, Chungnam National University, Daeduk Science Town, Daejeon 305-764, Republic of Korea
[b] Graduate of Analytical Science and Technology (GRAST), Chungnam National University, Daeduk Science Town, Daejeon 305-764, Republic of Korea

ARTICLE INFO

Article history:
Received 18 September 2010
Received in revised form
27 November 2010
Accepted 30 November 2010
Available online 7 December 2010

Keywords:
PMN–PT
Pulsed laser deposition
Heteroepitaxy
Ferroelectric properties
LNO/CeO_2/YSZ buffered Si substrate

ABSTRACT

Ferroelectric PMN–PT thin films with a thickness of 600 nm were epitaxially grown on buffered Si (0 0 1) substrates at a substrate temperature that ranged from 550 to 700 °C using pulsed laser deposition (PLD). $LaNiO_3$ (LNO) electrode thin films with a resistivity of ~1900 μΩ cm were epitaxially grown on CeO_2/YSZ buffered Si (0 0 1) substrates. The PMN–PT thin films grown at 600 °C on LNO/CeO_2/YSZ/Si substrates had a pure perovskite and epitaxial structure. The PMN–PT films exhibited a high dielectric constant of about 1818 and a low dissipation factor of 0.04 at a frequency of 10 kHz. Polarization-electric-field (P-E) hysteresis characteristics, with a remnant polarization of 11.1 $\mu C/cm^2$ and a coercive field of 43 kV/cm, were obtained in the epitaxial PMN–PT films.

1. Introduction

Ferroelectric thin films are of great interest due to a wide range of applications such as pyroelectric and piezoelectric sensors, microwave devices, micro-actuators, and most remarkably, nonvolatile random access memory (NVRAM). Among all types of ferroelectric materials, lead magnesium niobate and its solid solutions for lead titanate have been intensively investigated in recent years. A combination of 0.65 at.% of PMN with 0.35 at.% of PT is known as the morphotropic phase boundary (MPB) that separates the tetragonal and rhombohedral perovskite phases of $0.65Pb(Mg_{1/3}Nb_{2/3})O_3$–$0.35PbTiO_3$ (PMN–PT).

The use of silicon substrates with Pt as the bottom electrodes ($Pt/Ti/SiO_2/Si$) is common because of the good metallic properties and high oxidation resistance of Pt metal [1]. The epitaxial films are expected to exhibit improved properties compared to their randomly oriented polycrystalline film counterparts [2]. Little success has been achieved in obtaining high quality epitaxial perovskite PMN–PT films on a conductive electrode due to the appearance of stable pyrochlore phases. To achieve oriented, or even epitaxial films, the PMN–PT films are prepared on single crystal substrates, such as $SrTiO_3$ [3], Al_2O_3 [4], and $LaAlO_3$ [5], that posses a crystal structure and lattice constants that approximate those of PMN–PT. However, single-crystal substrates are expensive and can only provide a small-sized geometry, which is contrary to Si technology that features lower cost, a larger area, and volume production. Epitaxial PMN–PT films cannot be grown directly on a Si substrate due to a large lattice mismatch and a severe interface diffusion. In order to overcome these problems, structural templates and chemical buffer layers have been developed to grow high-quality, epitaxial, ferroelectric films on silicon substrates.

Among various buffer layer materials, metallic perovskite-type oxides, such as $La_{0.5}Sr_{0.5}CoO_3$ (LSCO) [6], $LaNiO_3$ (LNO) [7], $YBa_2Cu_3O_{7-\delta}$ (YBCO) [8], and $SrRuO_3$ (SRO) [9], have been used as the epitaxial template for the growth of ferroelectric films and bottom electrodes. For the selection of bottom electrodes, pseudocubic LNO, with a lattice parameter of 0.384 nm, is a conductive oxide that shows promise. Pseudocubic LNO has a crystal structure suitable for integration in epitaxial heterostructures with perovskites because of its good transport properties, simple composition, and excellent barrier properties that include good thermal stability.

Various deposition techniques such as solution–gelation [1], sputtering [4], electrophoretic deposition (EPD) [10], and pulse laser deposition (PLD) [5] have been used for the growth of PMN–PT thin films. PLD has emerged as an appropriate technique for obtaining films with a desired stoichiometry without post-deposition thermal treatment.

There are few reports on the preparation and electrical properties of epitaxial PMN–PT thin films on Si substrates with the use of suitable buffer layers [11,12]. To the best of our knowledge, this

* Corresponding author at: School of Nano Science and Technology, Chungnam National University, Daeduk Science Town, Daejeon 305-764, Republic of Korea. Tel.: +82 42 821 6638; fax: +82 42 822 3206.
E-mail address: sgyoon@cnu.ac.kr (S.-G. Yoon).

0925-8388/$ – see front matter © 2010 Elsevier B.V. All rights reserved.
doi:10.1016/j.jallcom.2010.11.200

Table 1
Deposition conditions of PMN–PT, LNO, CeO_2, and YSZ films grown on Si substrates.

Deposition parameters	YSZ	CeO_2	LNO	PMN–PT
Target	YSZ ceramics	CeO_2 ceramics	$LaNiO_3$ ceramics	0.65PMN–0.35PT single crystal
Deposition temperature (°C)	750	750	600	550–700
Film thickness (nm)	75	50	200	600
Deposition pressure (Torr)	5×10^{-4}	5×10^{-4}	0.3	0.3
Energy density (J/cm^2)	1.5	1.5	1.5	1.5
Target-substrate distance (cm)	8	8	6	6
Substrates	Si	YSZ/Si	CeO_2/YSZ/Si	LNO/CeO_2/YSZ/Si

is the first report on the epitaxial growth of PMN–PT thin films on LNO/CeO_2/YSZ-coated Si substrates using the PLD method. In the present study, 600-nm thick PMN–PT films were deposited on buffered Si (0 0 1) substrates at various substrates temperatures by pulsed laser deposition, and the electrical properties of the epitaxial PMN–PT films grown at 600 °C are discussed.

2. Experimental methods

The 0.65PMN–0.35PT/LNO/CeO_2/YSZ thin films were grown at a substrate temperature that ranged from 550 to 700 °C on Si (0 0 1) substrates by pulsed laser deposition (PLD) using a pulsed KrF excimer laser (248 nm, Lamda Physik COMPex-Pro 201). A PMN–PT single-crystal target with a diameter of 2.54 cm was used for deposition of the PMN–PT thin films. However, the sintered ceramic disks of $LaNiO_3$ (LNO), CeO_2, and $Y_{0.15}Zr_{0.85}O_{1.93}$ (YSZ) were used as the target for each buffer layer. The Si (0 0 1) substrates were attached to a heater plate by silver paste in order to maintain a uniform temperature. The details of the conditions for deposition of the PMN–PT/LNO/CeO_2/YSZ heterostructure onto Si substrates are summarized in Table 1. After deposition, high-purity oxygen was introduced into the growth chamber up to 300 Torr and then the films were cooled naturally to room temperature.

Film thicknesses were measured using cross-sectional scanning electron microscopy (SEM) images. The surface morphology and buffer layers of the PMN–PT films were studied by atomic force microscopy (AFM, AUTOPROBE CP, PSI). The phase, crystallinity and epitaxial relationships of the heterostructure were investigated by θ–2θ, ω-scan and Φ-scan, respectively, using a high-resolution X-ray diffraction (HRXRD, Rigaku RINT2000). The microstructure and the interface of the films were studied using high-resolution transmission electron microscopy (TEM: JEM-2100F). The elemental distributions in the PMN–PT/LNO/CeO_2/YSZ/Si structure were investigated using secondary ion mass spectroscopy (SIMS). The resistivity of the LNO thin films was measured by an electrometer (CMT-SR 1000) using a four-point probe.

For measurement of the electrical properties of the PMN–PT films, the Pt top electrodes were deposited onto the PMN–PT surface at room temperature by dc sputtering using an appropriate shadow mask. The polarization vs. electric field (P-E) curve of the films was measured using an RT66A ferroelectric tester (Radiant Technology) operated in the virtual ground mode. The dielectric constant and losses were obtained by impedance analysis with a HP4194A apparatus in frequencies that ranged from 100 Hz–1 MHz. Permittivity vs. field curves were also measured.

3. Results and discussion

Fig. 1 shows the XRD θ–2θ scans for PMN–PT films deposited on LNO/CeO_2/YSZ/Si at various temperatures ranging from 550 to 700 °C. The thicknesses of the PMN–PT films and LNO electrodes were maintained at 600 and 200 nm, respectively. The XRD patterns showed that the PMN–PT films as-grown at 600 °C were free of the pyrochlore phase and exhibited the (0 0 l) reflections from each of the respective layers. Films grown at 550 °C showed poor crystallinity, which included a pyrochlore phase. A mixture of the perovskite and the pyrochlore phase was observed at substrate temperatures above 650 °C. The peak intensity exhibiting the pyrochlore phase increased as the substrate temperature increased from 650 to 700 °C. Simultaneously, the films grown at a high deposition temperature showed deficient Pb and Mg concentrations because they were easily evaporated, and then the pyrochlore phase began forming with the perovskite phase [13]. However, at a low substrate temperature of 550 °C, the energy to crystallize the film into a complete perovskite phase was not sufficient, at which point the pyrochlore phase had already started to appear [14]. These results show that there is a narrow window of opportunity for the growth of PMN–PT thin films with a pure perovskite structure [15].

Fig. 2(a) shows the ω-scan (rocking curve) of the PMN–PT (0 0 2) and LNO (0 0 2) reflections in the case of the PMN–PT films deposited at 600 °C on an LNO/CeO_2/YSZ/Si substrate. The full width at half maximum (FWHM) corresponding to the PMN–PT and LNO was approximately 1.17° and 0.98°, respectively. In order to further determine the epitaxial relationship between the films and the substrate, phi scans of the hetero-structures were performed. Fig. 2(b) shows the phi scans of the PMN–PT (1 1 1), LNO (1 1 1), CeO_2 (1 1 1), YSZ (1 1 1) and Si (1 1 1), which are four-fold symmetry reflections exhibiting a typical cubic structure. These scans show that the CeO_2 and YSZ layers have a cube-on-cube epitaxial relationship to the Si substrate: (0 0 1) [1 0 0]CeO_2//(0 0 1)[1 0 0] YSZ//(0 0 1)[1 0 0]Si. The scans also show that the PMN–PT and the LNO layers have a 45°-rotated epitaxial relationship to the Si substrate: (0 0 1)[1 1 0]PMN–PT//(0 0 1)[1 1 0]LNO//(0 0 1)[1 0 0]Si. This was attributed to a low (0.1%) mismatch between the diagonal of the face of the LNO pseudocubic unit cell and the CeO_2 lattice parameter [16].

The epitaxial nature of each layer with respect to the Si substrate was further verified with a high-resolution TEM using the PMN–PT/LNO/CeO_2/YSZ heterostructure. Here, the PMN–PT films were grown at 600 °C. Fig. 3(a) shows a cross-sectional TEM image of each layer, indicating well-matched films with high density. The orientation was confirmed by the electron diffraction pattern (Fig. 3b), which indicated that each layer showed an epitaxial relationship.

Figs. 4(a) and (b) shows the AFM three-dimensional images of the LNO films grown on CeO_2/YSZ/Si and the PMN–PT films grown on LNO/YSZ/CeO_2/Si, respectively. The 200-nm thick LNO film showed an extremely smooth structure with a root mean square (rms) roughness of about 1.9 nm, showing promise for the subsequent growth of the defect-free ferroelectric thin films. The resistivity of the epitaxial LNO films was approximately 1900 μΩ cm. Moreover, the rms roughness of the 600-nm thick

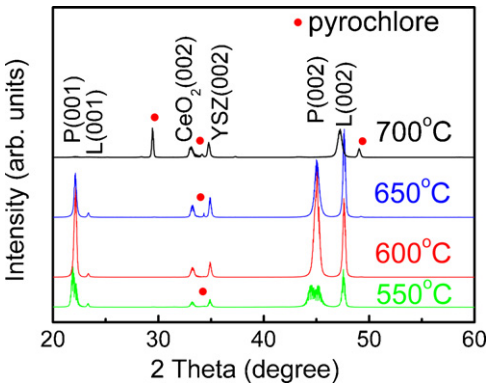

Fig. 1. XRD θ–2θ patterns of 0.65PMN–0.35PT/LNO/CeO_2/YSZ/Si (0 0 1) thin films as-grown at various substrate temperatures (550–700 °C) in an oxygen ambient of 300 mTorr.

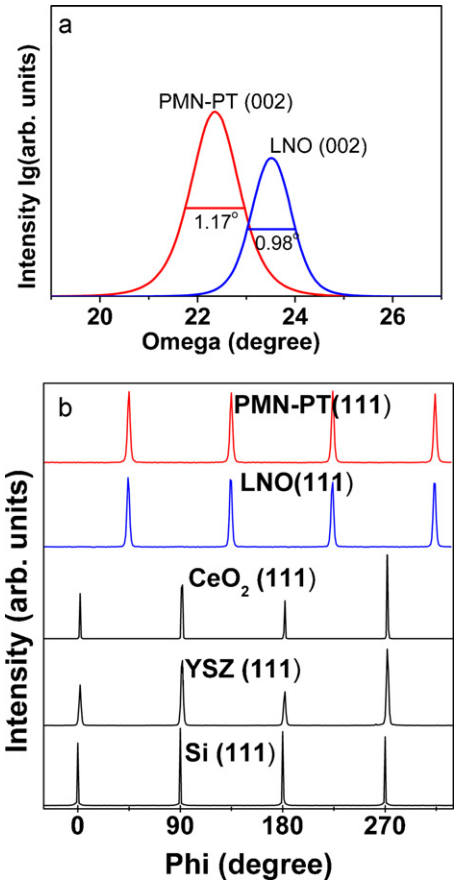

Fig. 2. (a) Rocking curves of the PMN–PT (0 0 2) and the LNO (0 0 2) and (b) Phi scans of the PMN–PT (1 1 1), LNO (1 1 1), CeO_2 (1 1 1), YSZ (1 1 1), and Si (1 1 1) plane.

PMN–PT films grown on an LNO bottom electrode was approximately 5.9 nm.

The homogeneity of each layer in the grown films was confirmed using the SIMS. Fig. 5 shows the SIMS depth profiles of the PMN–PT/LNO/CeO_2/YSZ heterostructure. The ion-count profiles of Pb, Mg, Nb and Ti showed a uniform compositional distribution in the PMN–PT layer. The depth profiles of the lanthanum and the nickel in the LNO film showed a slight diffusion into the PMN–PT layer. However, it should be noted that the LNO layer effec-

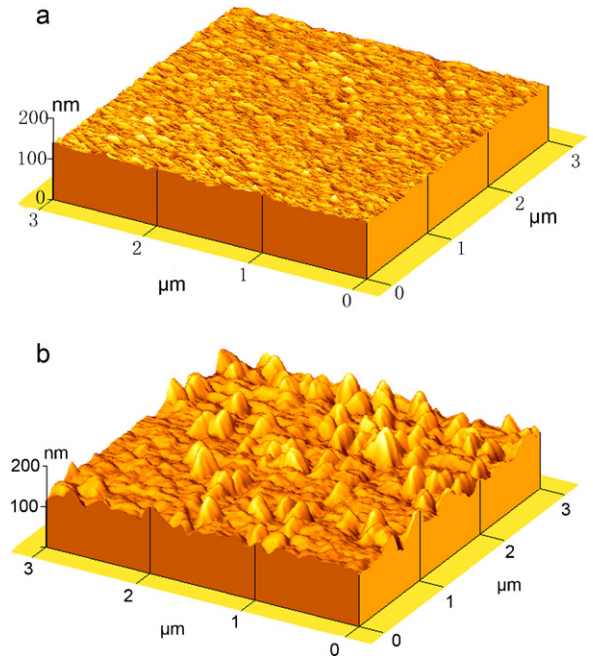

Fig. 4. AFM three-dimensional images over 3 μm × 3 μm of (a) 200-nm thick epitaxial LNO film grown on CeO_2/YSZ buffered Si substrate and (b) 600-nm thick PMN–PT film grown on the LNO.

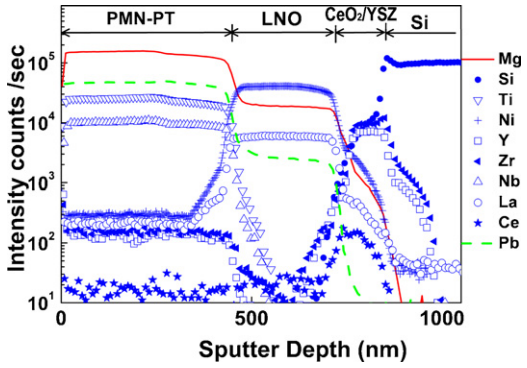

Fig. 5. SIMS depth-profile of the PMN–PT/LNO/CeO_2/YSZ/Si stacked layer.

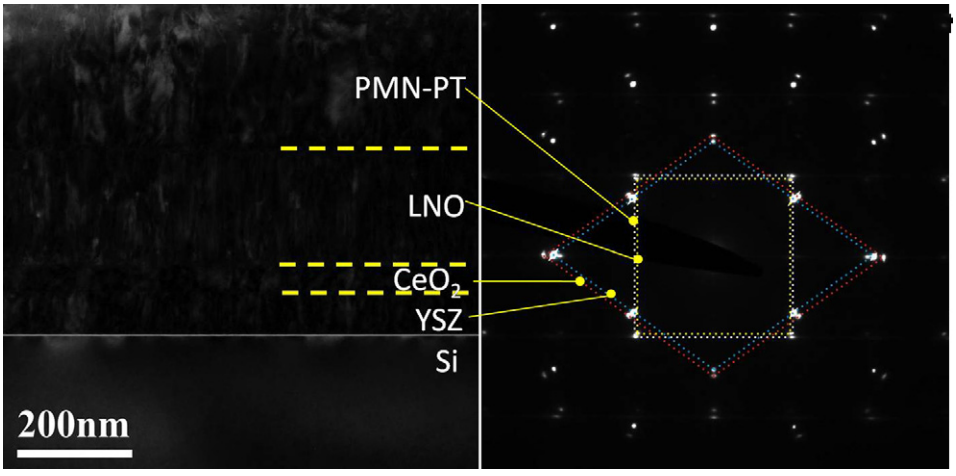

Fig. 3. (a) Cross-sectional TEM image of the PMN–PT/LNO/CeO_2/YSZ/Si stacked layers and (b) the nano-beam electron diffraction pattern observed from the [0 1 0] direction at each layer. The PMN–PT films were grown at 600 °C.

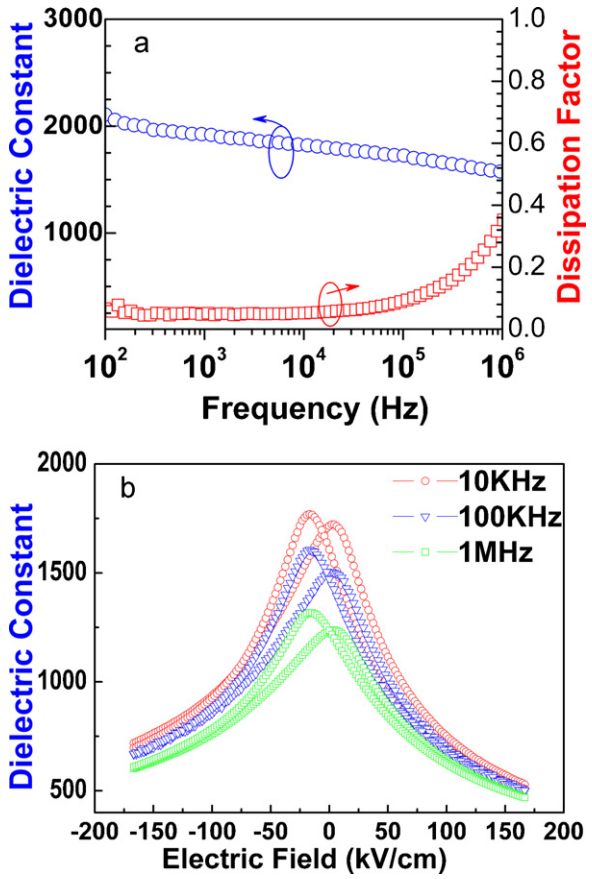

Fig. 6. (a) Frequency dependence on the dielectric constant and the dissipation factor in the epitaxial PMN–PT films grown at 600 °C. (b) Dielectric constant vs. electric field characteristics of the PMN–PT capacitor measured at different frequencies.

tively blocked the inter-diffusion and chemical reaction between the PMN–PT and the buffer layers.

The dielectric constant (ε_r) and the dissipation factor ($\tan\delta$) were measured as a function of frequencies that ranged from 100 Hz to 1 MHz, as shown in Fig. 6(a). The PMN–PT films grown at 600 °C showed a dielectric constant of about 1818 at 10 kHz, which was high when compared with the published results [13,15,17]. The dissipation factor did not exceed 0.06 between 100 Hz and 100 kHz. However, a sharp increase in the dissipation factor above 100 kHz was observed and the result was attributed to the high resistivity of the LNO bottom electrode (1900 μΩ cm). The increase in losses at high frequencies is an artifact that is due to the limited conductivity of the oxide bottom electrode.

Fig. 6(b) displays the dependence of the dielectric constant as a function of the electric field (ε_r-E) of Pt/PMN–PT/LNO/CeO_2/YSZ/Si capacitors. During the sweep up and down of the dc bias voltage, the dielectric constant showed a maximum value in the vicinity of the switching of the spontaneous polarization. Therefore, two maxima, which were due to ferroelectric polarization reversals, were clearly seen in the sweep up and down processes. Further, ε_r-E characteristics were found to be asymmetric in nature owing to the different top and bottom electrodes. The various reasons – the presence of different chemical defects on both interfaces [18] and different electrode material used for the contacts [19] – must be considered when accounting for the asymmetric characteristics of the dielectric constant-electric field.

Fig. 7 shows the P-E hysteresis loop of the epitaxial PMN–PT/LNO/CeO_2/YSZ/Si films taken at a frequency of 1 kHz using the Pt (100 μm diameter) as the top electrode. A good hysteresis characteristic of the remnant polarization (P_r) of 11.1 μC/cm^2

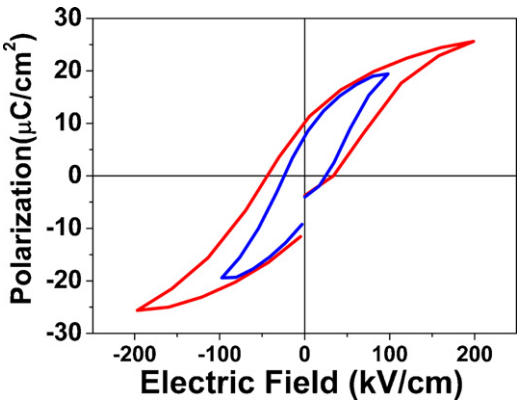

Fig. 7. Polarization-electric field (P-E) hysteresis loop of the PMN–PT thin films grown at 600 °C.

and a coercive field (E_c) of 43 kV/cm was observed under an electric field of 200 kV/cm. The P_r value of the optimized PMN–PT/LNO films on buffered Si substrates in the present study was significantly higher than that of the oriented PMN–PT film on LNO coated SiO_2/Si (P_r, 8 μC/cm^2) [17]. They are also comparable to that of epitaxial PMN–PT films grown on an MgO/TiN-buffered Si substrate (P_r, 9 μC/cm^2) [20] and even the epitaxial PMN–PT film grown on an LAO single-crystal substrate (P_r, 12 μC/cm^2) [13]. The high polarization values obtained in this work are possibly due to the excellent epitaxial quality of the PMN–PT films grown on the tri-layer buffered Si substrates, which indicates that LNO/CeO_2/YSZ/Si can be used as an appropriate structure for the epitaxial growth of PMN–PT films. Moreover, the obtained ferroelectric properties of the epitaxial PMN–PT films on buffered Si are comparable to those of epitaxial $Pb(Zr_{0.53}Ti_{0.47})O_3$ of MPB composition on buffered Si (P_r, 10 μC/cm^2) [21]. Further work is needed to improve the ferroelectric properties of these kinds of heterostructures, which show promise for application to ferroelectric memory and other microelectronic elements.

The above-mentioned electrical properties are inferior to those of the PMN–PT sintered bodies and single crystals. A possible reason could be the effect of the grain size associated with the stabilization of intermediate sub-micrometer/nanoscale polar domain configurations [22]. In addition, Maria et al. [9] demonstrated that if a better lattice-matched substrate/electrode/film system were used, electrical properties similar to those of single crystals could be realized. Other effects, such as substrate clamping, and residual strain may also contribute to the electrical values that are lower than those of the films grown on a single-crystal substrate.

4. Conclusions

The 600-nm thick perovskite PMN–PT films on LNO/CeO_2/YSZ tri-layer buffered Si (0 0 1) substrates were epitaxially grown at 600 °C by PLD technique. XRD and high-resolution TEM study of the PMN–PT and LNO films revealed that the CeO_2 and YSZ layers have a cube-on-cube epitaxial relationship to the Si substrate and a 45°-rotated epitaxial relationship to the PMN–PT and LNO films. The LNO films have a smooth surface with an rms roughness of 1.9 nm, which are favorable for the growth of defect-free over-layers. The capacitors showed a dielectric constant of 1818 and a dissipation factor of 0.04 at 10 kHz. The hysteresis loop for the pyrochlore-free PMN–PT films demonstrated the ferroelectric behavior of the films with a remnant polarization of 11.1 μC/cm^2 and a coercive field of 43 kV/cm. The present study showed excellent epitaxial growth of PMN–PT films on an LNO/CeO_2/YSZ/Si substrate with an improved ferroelectric behavior.

Acknowledgements

This work was funded by a Korea Science and Engineering Foundation (KOSEF) grant funded by the Korea government (MOST) (R01-2007-000-21017-0), and by a KOSEF grant funded by the Korean Government (MEST) (No. 2009-0079164). This work is also the outcome of a Manpower Development Program for Energy & Resources supported by the Ministry of Knowledge and Economy (MKE), and was supported by the Brain Korea 21 Project in 2006.

References

[1] M. Feng, W. Wang, H. Ke, J.C. Rao, Y. Zhou, J. Alloys Compd. 495 (2010) 154–157.
[2] R. Ramesh, D.G. Schlom, Science 296 (2002) 1975–1976.
[3] B.T. Liu, C.S. Cheng, F. Li, D.Q. Wu, X.H. Li, Q.X. Zhao, Z. Yan, X.Y. Zhang, J. Alloys Compd. 440 (2007) 276–280.
[4] L. Krishna, M. Sunder, P.D. Moran, J. Electron. Mater. 39 (2010) 132–137.
[5] A.R. Chaudhuri, S.B. Krupanidhi, P. Mandal, A. Sundaresan, J. Appl. Phys. 106 (2009) 054103.
[6] A.S. Asha, M.T. Sebastian, M.K. Jayaraj, J. Alloys Compd. 449 (2008) 68–72.
[7] Y.H. Yu, M.O. Lai, L. Lu, P. Yang, J. Alloys Compd. 449 (2008) 56–59.
[8] I. Yamaguchi, T. Manabe, M. Sohma, K. Tsukada, W. Kondo, K. Kamiya, S. Mizuta, T. Kumagai, IEEE Trans. Appl. Supercon. 15 (2005) 2927–2930.
[9] J.P. Maria, W. Hackenberger, S. Trolier-McKinstry, J. Appl. Phys. 84 (1998) 5147–5154.
[10] J. Chen, H. Fan, X. Chen, P. Fang, C. Yang, S. Qiu, J. Alloys Compd. 471 (2009) L51–L53.
[11] T. Kiguchi, N. Wakiya, K. Shinozaki, T.J. Konno, Mater. Sci. Eng. B-Adv. 161 (2009) 160–165.
[12] D.S. Tsvetkov, A.Y. Zuev, A.I. Vylkov, A.N. Petrov, Solid State Ionics 178 (2007) 1458–1462.
[13] J. Wang, K.H. Wong, H.L.W. Chan, C.L. Choy, Appl. Phys. A-Mater. 79 (2004) 551–556.
[14] Z. Huang, Q. Zhang, R.W. Whatmore, J. Appl. Phys. 86 (1999) 1662–1669.
[15] F. Wu, X.M. Li, W.D. Yu, X.D. Gao, X. Zhang, Appl. Phys. A-Mater. 88 (2007) 781–784.
[16] T.W. Chiu, N. Wakiya, K. Shinozaki, N. Mizutani, Thin Solid Films 426 (2003) 62–67.
[17] R. Herdier, M. Detalle, D. Jenkins, D. Remiens, D. Grebille, R. Bouregba, J. Cryst. Growth 311 (2008) 123–127.
[18] F.K. Chai, J.R. Brews, R.D. Schrimpf, D.P. Birnie Iii, J. Appl. Phys. 82 (1997) 2505–2516.
[19] T. Kawakubo, K. Abe, S. Komatsu, K. Sano, N. Yanase, IEEE Electron. Dev. Lett. 18 (1997) 529–531.
[20] H.Y. Cheung, F.F. Hau, J. Wang, K.H. Wong, Ferroelectrics 260 (2001) 219–224.
[21] C. Wang, D.E. Laughlin, M.H. Kryder, Appl. Phys. Lett. 90 (2007) 172903–172913.
[22] M. Alguero, M. Stewart, M.G. Cain, P. Ramos, J. Ricote, M.L. Calzada, J. Phys. D: Appl. Phys. 43 (2010) 205401–205406.